38th International Electric Vehicle Symposium and Exhibition (EVS38) Göteborg, Sweden, June 15-18, 2025

Challenges and Innovations in Designing Axial Flux Electrical Machines for Automotive Traction Applications

Kristoffer Nilsson[1*], Hans Johansson[1], Johan Nilsson[1], Jana Schumacher[1], Sven Kalkan[1], Meng Lu[1], Pontus Fyhr[1, 2]

[1*]*corresponding author, Alvier Mechatronics, Helsingborg Sweden, kristoffer.nilsson@alviermechatronics.com*

[2]*Lund University, Lund Sweden*

Executive Summary

While the electromagnetic design and optimization of automotive traction motors pose significant challenges, achieving accurate and reliable results for axial flux traction machines introduces an additional layer of complexity. Yet, the journey from a robust electromagnetic concept to a fully functional machine involves more than just optimization; it requires addressing an array of practical engineering and manufacturing challenges. The transition from concept to product reveals critical hurdles in areas beyond the electromagnetic domain, such as bearing solutions, assembly processes, tooling requirements, manufacturing tolerances, material selection, insulation system and test specifications. Each of these elements requires careful consideration to ensure a machine that not only performs as intended but is also feasible to manufacture and build in a repeatable and efficient manner.

Keywords: Automotive, Axial Flux, Traction Motor, SMC, Adhesives

1 Introduction

The increasing demand for high-efficiency, compact, and lightweight electric propulsion systems in automotive applications has spurred significant interest in axial flux machines. Compared to conventional radial flux machines, axial flux machines [1] can offer higher torque density and improved power-to-weight ratios, making them particularly attractive for electric vehicle traction applications. However, the design and manufacturing of axial flux machines present unique challenges, ranging from complex electromagnetic modelling to stringent mechanical tolerances, manufacturing processes and advanced thermal management.

Many publications cover the electromagnetic design and optimization of axial flux machines and quite a few companies now offer high performance axial flux machines produced in increasing volumes. The field of mechanical design, manufacturing and assembly of axial flux machines is however scarcer in the number of publications. With this white paper we are aiming to add to the knowledge about engineering, assembly and manufacturing challenges and potential solutions to them. This paper contains a few selected engineering challenges ranging from adhesive selection to magnet segmentation encountered in the journey from an electromagnetic concept to a working machine. Some solutions presented would be scalable to mass production while others would need to be re-engineered or optimized to be able to scale.

2 Methodology

The concept design started with electromagnetic, thermal and mechanical simulations in parallel with mechanical design and the development of a 3D-CAD model. In the detailed design further analysis was performed in parallel with reviews with key suppliers. In order to de-risk the project, several component and sub-system tests were planned and performed before the final full motor build. This includes for example adhesive testing, rotor burst test and trial magnetization.

2.1 Machine concept

The presented machine is a dual rotor single stator topology with 24 teeth and 20 poles, concentrated winding and direct oil cooling for both the rotor and stator. It is depicted in Figure 1.

Figure 1: CAD rendering of the axial machine stator and rotor cross section.

2.2 Rotor

The rotor is made up from two rotor discs mounted on a hub. The rotor discs are made from a steel disc, a rotor back iron and magnets. Shims are used to achieve enough accuracy for the air gap. For the rotor back iron two main alternatives were considered, SMC and coils from laminated electrical steel. Although SMC performed very well in the electromagnetic simulations it was not possible to find a mechanically sound design for the rotor using SMC due to the low tensile strength and brittle nature. Therefore, a coil from laminated electrical steel was chosen as back iron. As the rotor iron losses are typically less dominant than stator iron losses due to less high-frequency variations in the magnetic field in the rotor, it's typically not necessary to use a low loss grade or very thin laminations to reduce eddy currents. In this case an electrical steel with a thickness of 0.50 mm from the grade M330-50A with coating Remisol EB 5308K C5 was selected. The coils were vacuum epoxy infused using Veropal 582-1K4 after winding to increase the mechanical strength.

The laminated coils can optionally be ground to improve on mechanical tolerances which helps to keep control of the air gap and the glue gaps. Ground laminated coils can fulfil a flatness requirement of 0.05 mm, while the non-ground can fulfil a 0.40 mm flatness requirement. After the grinding the laminated coils can also optionally be blasted to improve the adhesive strength against the magnets. Any mechanical process will however impact the electromagnetic properties of soft magnetic materials. To understand the magnitude of the impact of these additional process steps a BH-Curve and loss measurement was performed in each state using a Brockhaus MPG200, as depicted in Figure 2 and Figure 3.

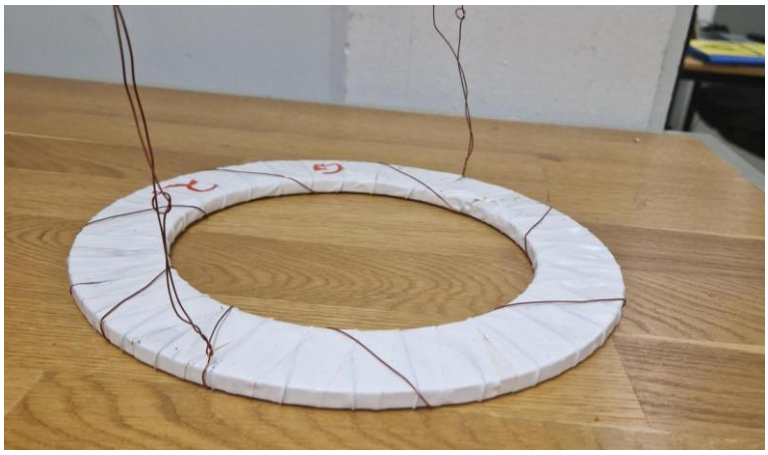

Figure 2: Rotor Laminated Back Iron Ring insulated and wound for BH and loss measurements.

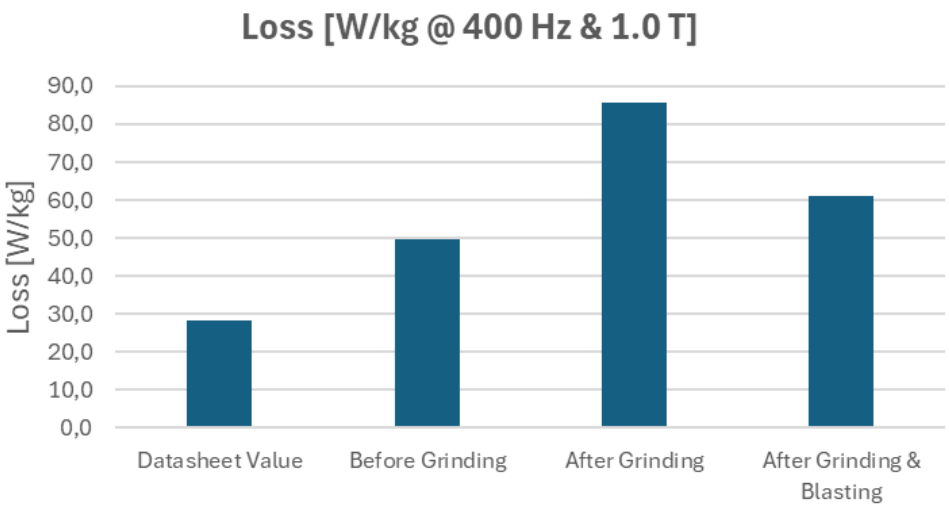

Figure 3: Results from loss measurements at different process stages.

Based on the BH and loss measurements, the improved mechanical tolerances and better adhesion the grinded and blasted version was used for the motor build. Based on the machine optimization and demag analysis N48SH magnets were selected for the design. As the magnets are exposed to a highly variable flux in the air gap segmentation is necessary to keep losses to a manageable level. In this design the thermal limit is determined by the magnet adhesive rather than the magnet itself. Lowering losses by segmentation and direct rotor oil cooling helps to keep the temperatures down below the 85°C limit set for the adhesive.

For good adhesion it's important to select the right coating on the magnets. For the iDS AX epoxy coated magnets were selected due to a supplier recommendation of best compatibility with the selected adhesive. The bonding strength was later confirmed by testing.

Magnet segmentation can add quite significant costs which means finding the right loss/cost balance for each application is important. Each additional segment also adds an adhesive gap, which reduces the effective magnet area/volume and thus the magnet strength.

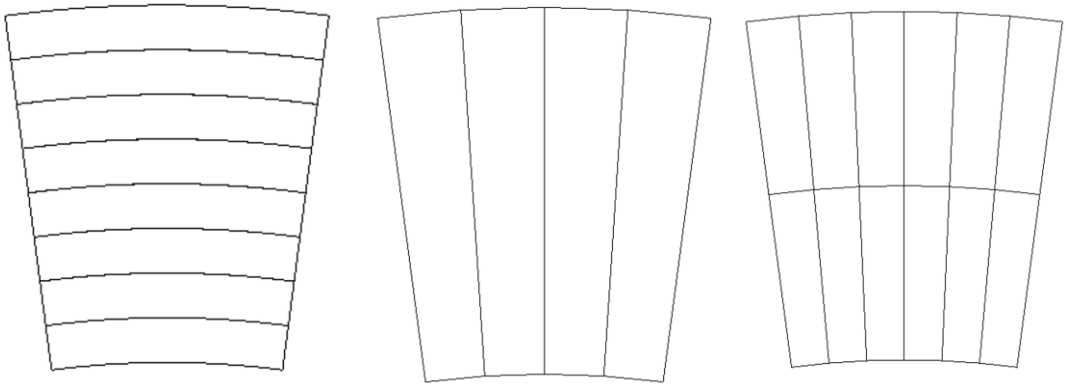

Figure 4: Basic types of magnet segmentation considered. From the left: circumferential, radial and combined.

Simulations were performed comparing the three different segmentation types as shown above and for 4, 6 and 8 segments, as depicted in Figure 4. The combined radial and circumferential segmentations as this variant give a larger area for the eddy currents to circulate. As can be seen in the plot below the losses decrease with the number of segments, but with diminishing returns for each additional segment, see Figure 5. For the selected segmentation the simulations were expanded in steps up to 24 segments, and 8 segments was selected as a balance between losses, cost and magnet strength, these trade-offs are depicted in Figures 6-8.

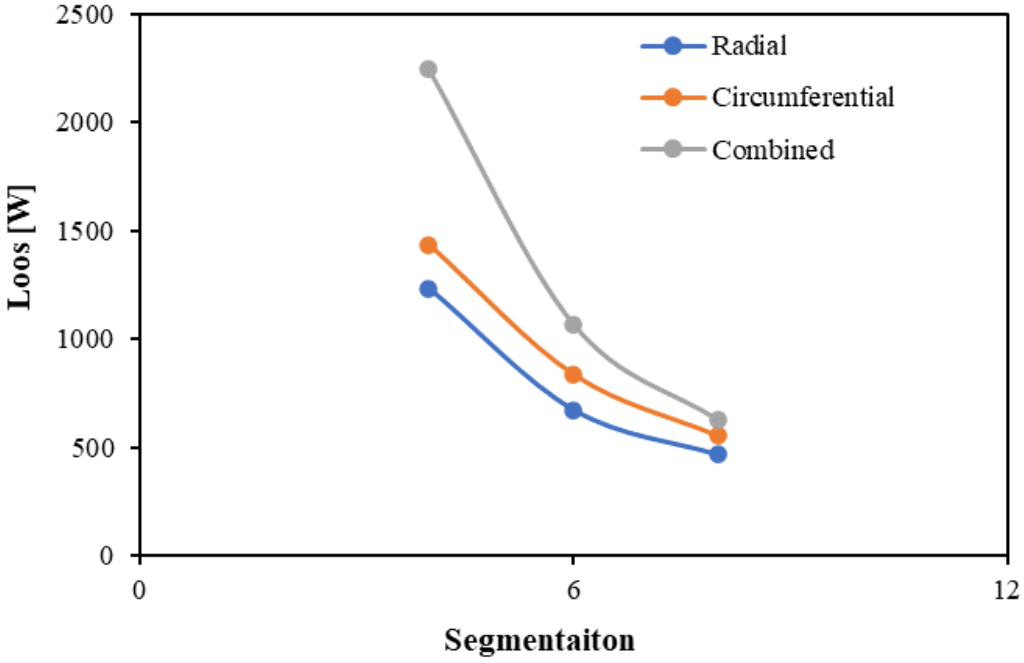

Figure 5: Losses vs number of segments for the three types of segmentations considered.

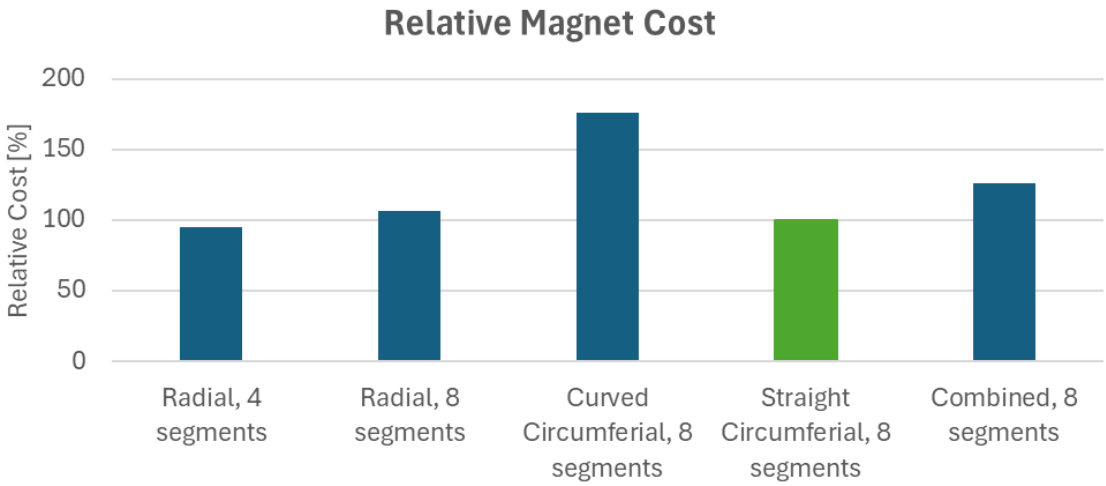

Figure 6: Relative cost for a few different types of segmentation. Green indicates the selected segmentation

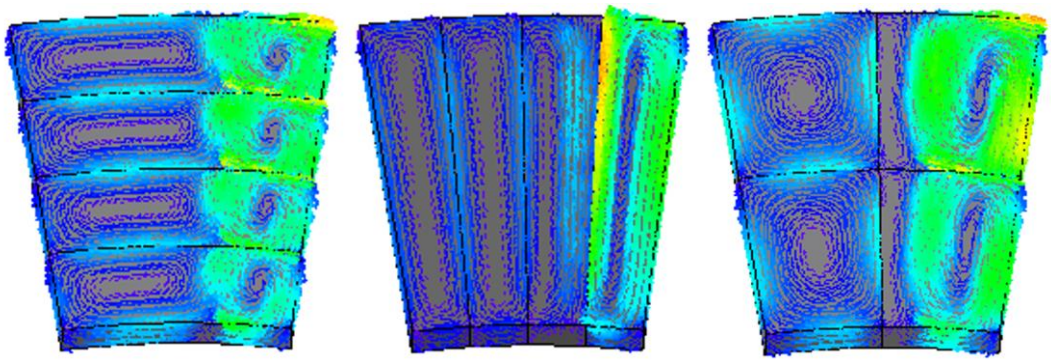

Figure 7: Eddy current density for three selected types of segmentations.

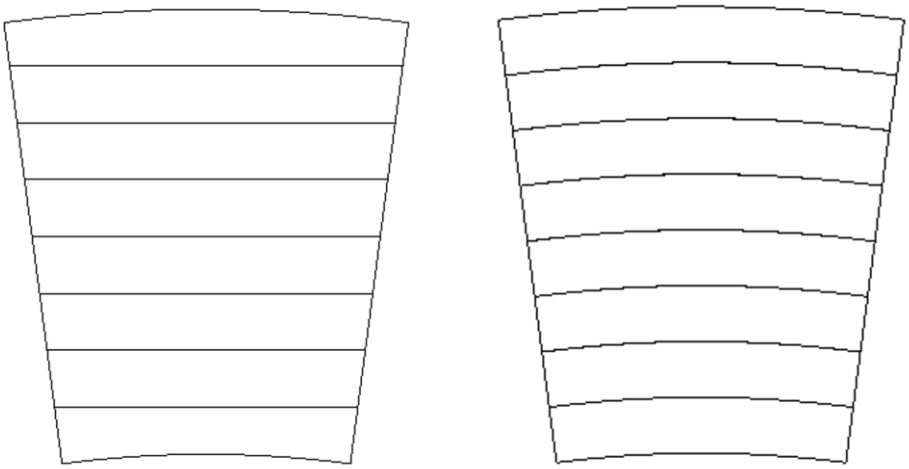

Figure 8: Cost optimized segmentation (straight cuts) vs original segmentation.

For prototype builds there are generally two options for magnetization, either build the machine with pre-magnetized magnets or build with non-magnetized magnets and magnetize the complete rotor after build. For the iDS AX the complete rotor magnetization was selected as it made the fixturing during the rotor build simpler and the process is also more similar to a typical volume manufacturing process. When using full rotor magnetization, it's important to consider the magnetization process and tooling early in the concept phase as this may impact the design, for example limiting the minimum distance between the magnets to give enough space for the magnetizing coils.

2.2.1 Rotor magnet adhesive selection

Selecting the right adhesive for the rotor magnets is a long and complex process involving a multitude of considerations. Firstly, due to the high-speed operation of the machine high strength is needed. A first screening was performed based on datasheet values for adhesion to steel. As the rotor operates at elevated temperatures up to 100°C the second step was to check the drop in strength over temperature. Quite a few adhesive candidates were dropped because their strength was declining sharply above 60-80°C. The third selection criteria was the Young's modulus. The Young's modulus over the operating temperature range should preferably not be too high as that will create more stress concentrations than a somewhat softer adhesive that will distribute the stresses more evenly. The fourth criteria to be checked was chemical compatibility with the rotor coolant oil. Most datasheet provides only a generic list of chemical compatibility, but that was used as a first indication of potential compatibility with the oil used in the iDS AX. A fifth selection criteria was the thermal conductivity, where a higher value is preferred to transport the heat from the magnet losses to the laminated back-iron which is oil cooled. A sixth selection criteria was the thermal expansion coefficient, where a value more similar to that of steel and FeNdB-Magnets is preferable to reduce the thermally induced stresses in the rotor. The properties influencing the selection of adhesive are listed in Table 1, and the temperature dependence of one adhesive is depicted in Figure 9.

Table 1: Selected key properties for considered adhesives

Adhesive Brand & Type	**Shear Strength Steel [MPa]**	**Shear Strength Aluminium [MPa]**	**Shear Strength Epoxy [MPa]**	**Tensile Modulus [GPa]**	**Thermal Conductivity [W/m*K]**	**Oil Compatibility**
Permabond ES 558	27-41	17-31	n/a	3.50	0.55	Yes
Permabond ES 562	20-35	14-27	n/a	2.10	0.25	Yes
Loctite EA 9514	45	40	24	1.46	0.30	Yes
Loctite EA 9497	20	15	8	2.42	1.40	Yes
Delo Monopox HT2999	45	16	n/a	4.40	0.40	n/a
Elan-Tech ASM 030	16-20	16-19	n/a	n/a	n/a	n/a
3M DP-76050N	n/a	30	n/a	5.97	n/a	n/a
Araldite 2014-1	17	18	8	4.00	n/a	Yes

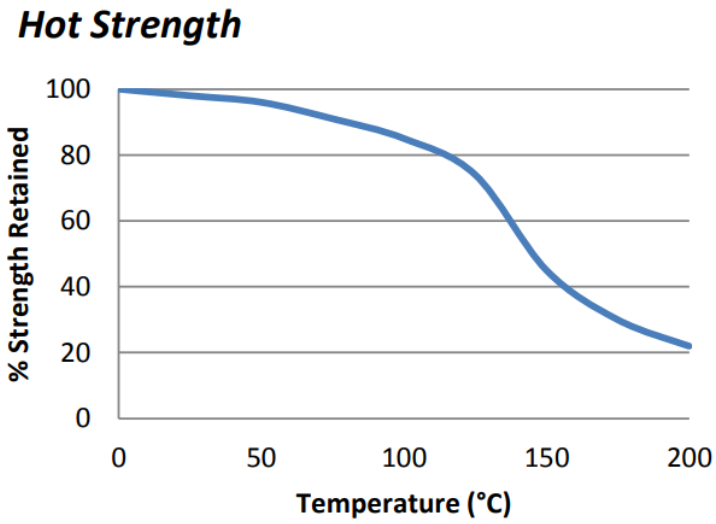

Figure 9: Example of drop in adhesive strength over temperature for Permabond ES558.

The next step in the adhesive selection process relates to the properties needed for the application and curing processes. First the list of adhesive candidates was down-selected based on their viscosity, temperature dependence of the viscosity and their thixotropic behaviour to ensure a smooth and even application, and a good flow and filling the adhesive gap. Many datasheets give the viscosity both as a number and as an analogy like “flows like solder” or “flows like water” or “paste” which can be helpful in the selection. Finally, the list was further down-selected based on the curing requirements for the adhesives. Here single component heat curing adhesives were preferred over two-component adhesives due to the simpler process in application of the adhesive for prototypes.

Table 2: Curing properties for the adhesives considered.

Adhesive Brand & Type	**Curing**	**Viscosity @ Room Temperature [mPa*s]**	**Flowability during curing**	**Thixotropic**
Permabond ES 558	Heat Curing	100 000-300 000	“flows like solder”	n/a
Permabond ES 562	Heat Curing	15 000-30 000	“self-levelling, flows like water”	n/a
Loctite EA 9514	Heat Curing	30 000-60 000	“gap-filling and sag resistant properties”	n/a
Loctite EA 9497	2K	8 000-24 000	“medium viscosity”	n/a
Delo Monopox HT2999	Heat Curing	400 000	n/a	Yes
Elan-Tech ASM 030	Heat Curing	400 000-650 000	n/a	n/a
3M DP-76050N	2K	n/a	n/a	n/a
Araldite 2014-1	2K	100 000	“paste”	Yes

As can be seen in the Table *1* and Table *2* above the data is often incomplete and there is no single adhesive that excels in all aspects, which makes supplier recommendations, experience from previous projects and testing key input to the final decision. Starting with a shortlist of a few potential candidates from the screening above testing was performed to confirm or reject each candidate based on shear strength, tear strength, Young’s Modules and feasibility in the application process.

The three down-selected candidates for the rotor glue were Permabond ES 558, Loctite EA 9514 and Delo Monopox HT2999. After application and curing tests, it was concluded that the Loctite EA 9514 does not flow as needed in this application and it was thus not included in the further testing. Permabond ES 558 and the Delo Monopox HT2999 were subject to tensile strength test, tear off adhesion strength test, modulus of elasticity test and torsional shear strength test. All the tests were conducted at room temperature, 80°C, 100°C and 120°C. The tests were conducted on magnets, laminated rotor back iron and rotor disc steel to get a good understanding of the adhesion to the different materials in the rotor. The results of these tests are depicted in Figures 10-12.

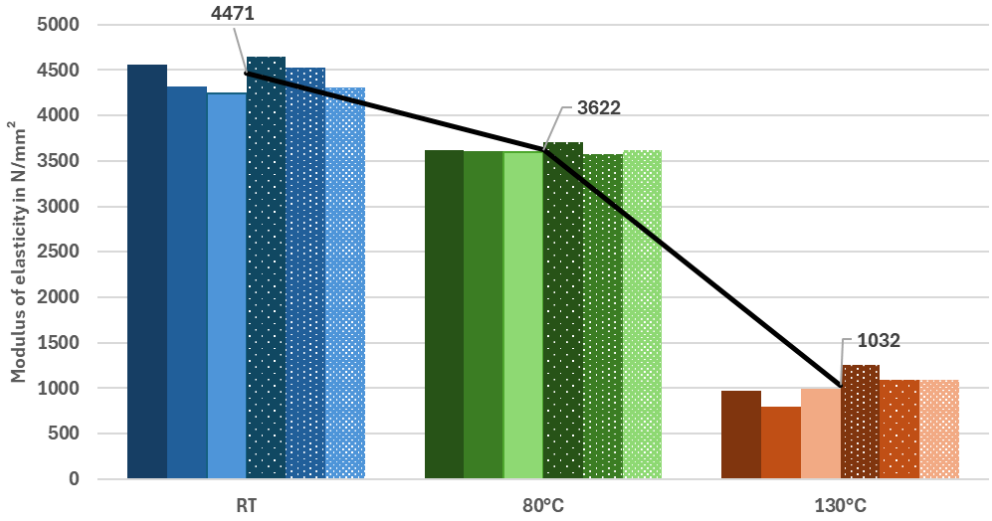

Figure 10: Permabond ES558 Youngs Modulus test results for five samples at each temperature.

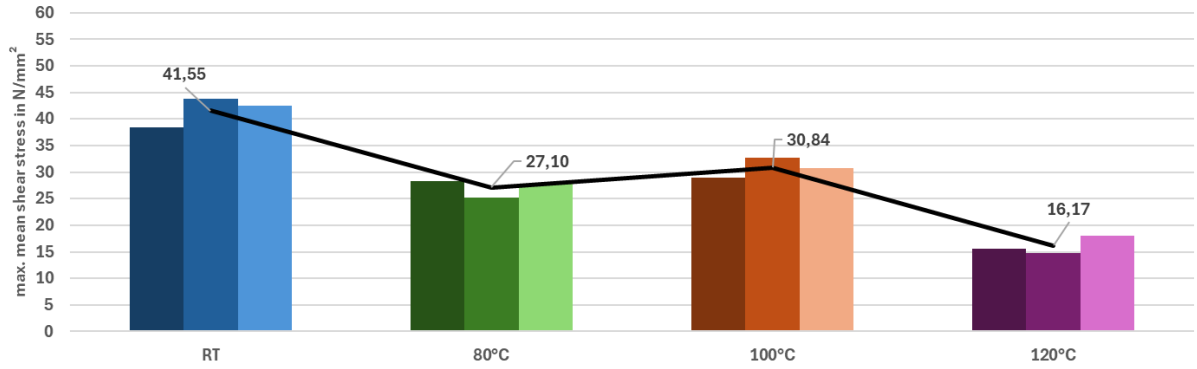

Figure 11: Torsional Shear Stress for Permabond ES 558 against the magnets for three samples of each.

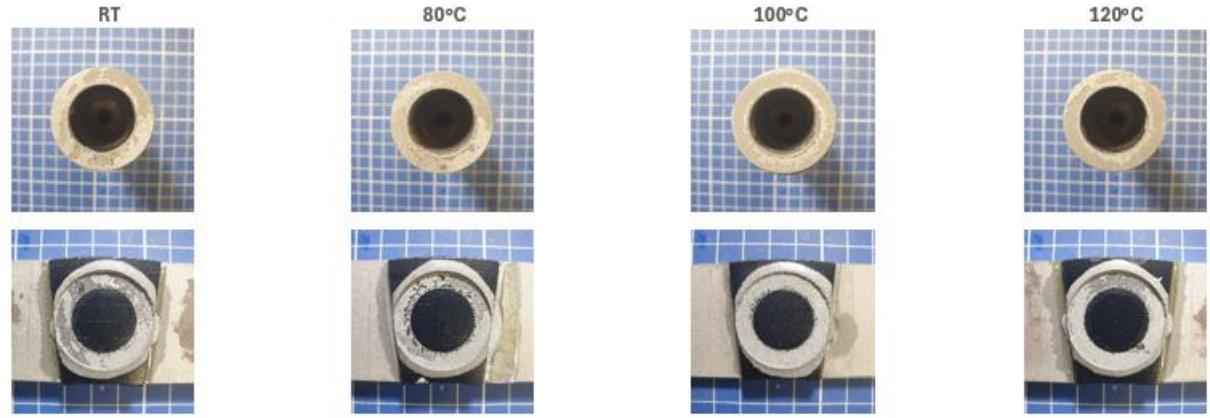

Figure 12: Adhesive joints after the test. Detailed inspection can give good clues to the exact failure mechanism.

Finally, the Permabond ES 558 was selected for the rotor due to good hot strength, decent to good values on other properties and a very good result in the application and curing tests.

As a preparation for the rotor build and related process development tests were performed with different glue gaps to understand the behaviour of Permabond ES 558 during heat curing. The tests were performed using sample epoxy glass fibre sheets and shims to vary the glue gap. The conclusion from these tests were that a target glue gap in the range of 0.10-0.20 mm is optimal. The results are depicted in Figures 13-16.

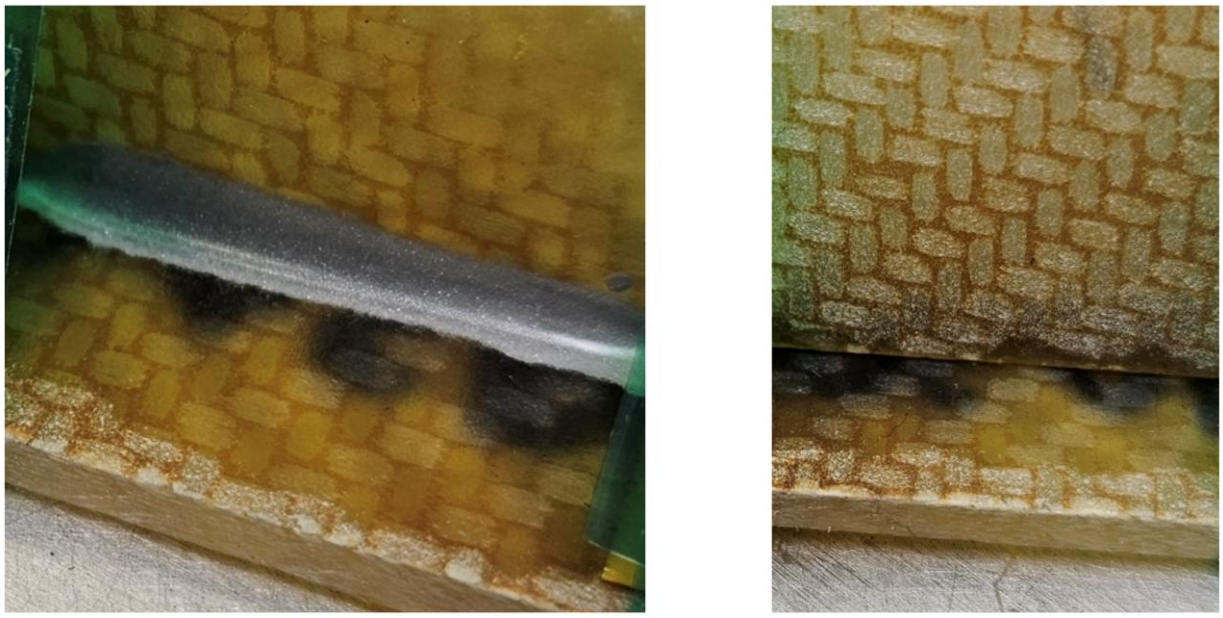

Figure 13: Adhesive joint on the upper side (left) and the underside (right) after curing with 0.05 mm glue gap. The joint has a nice radius on the upper side but has not fully penetrated to the underside.

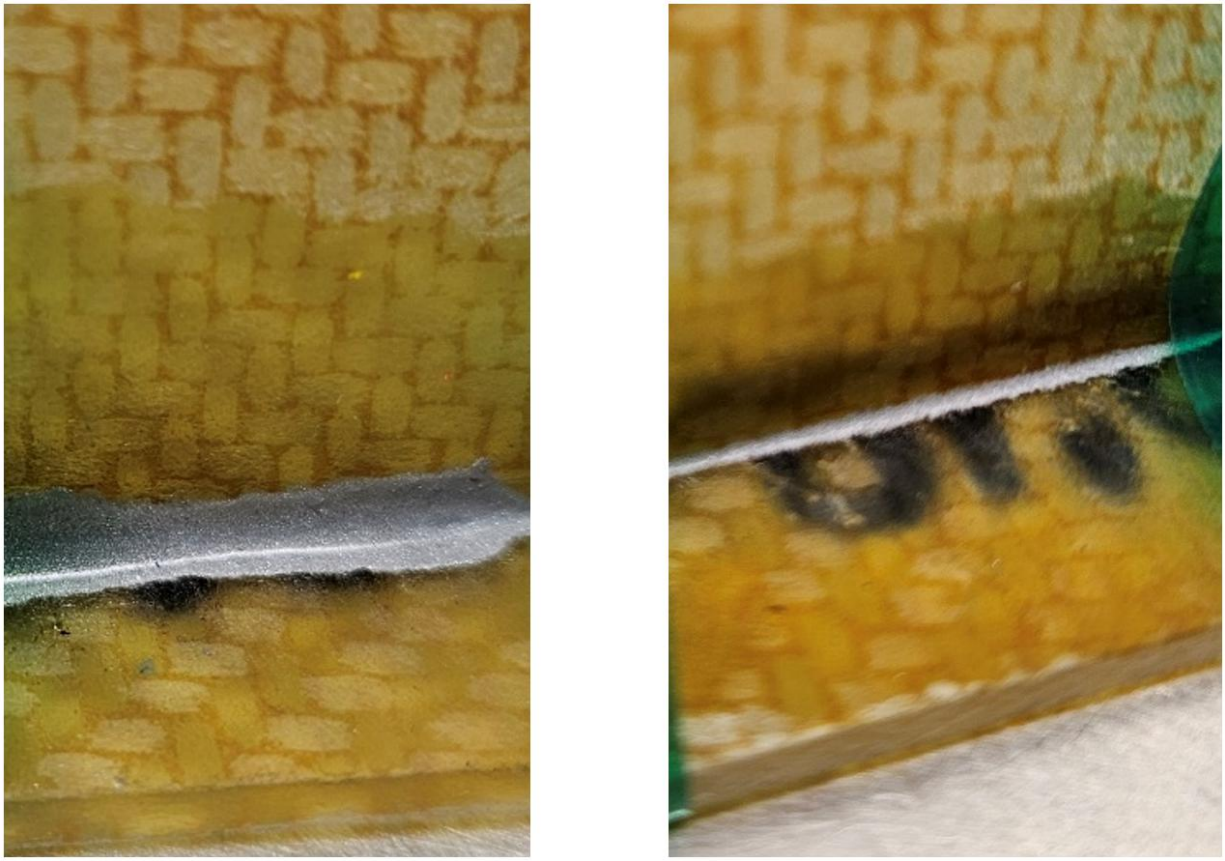

Figure 14: Adheive joint on the upper side (left) and the underside (right) after curing with 0.10 mm glue gap. The joint has a nice radius on the upperside, has penetrated the glue gap fully and formed a small radius on the underside.

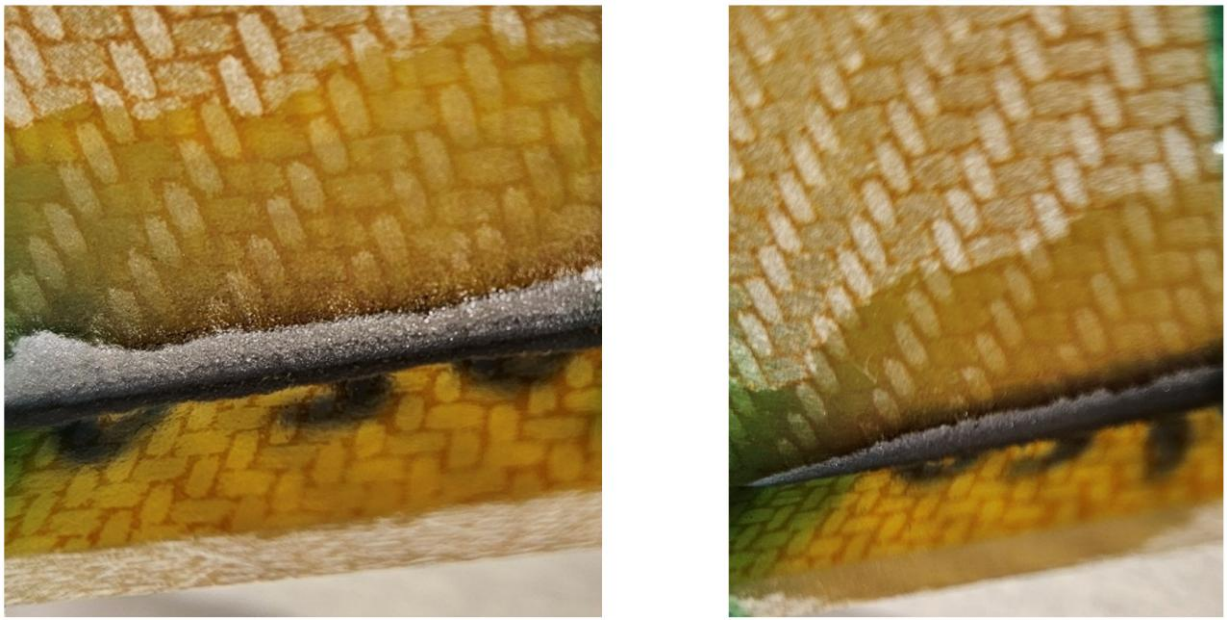

Figure 15: Adheive joint on the upper side (left) and the underside (right) after curing with 0.20 mm glue gap. The joint has a nice radius on the upperside, has penetrated the glue gap fully and formed a small radius on the underside.

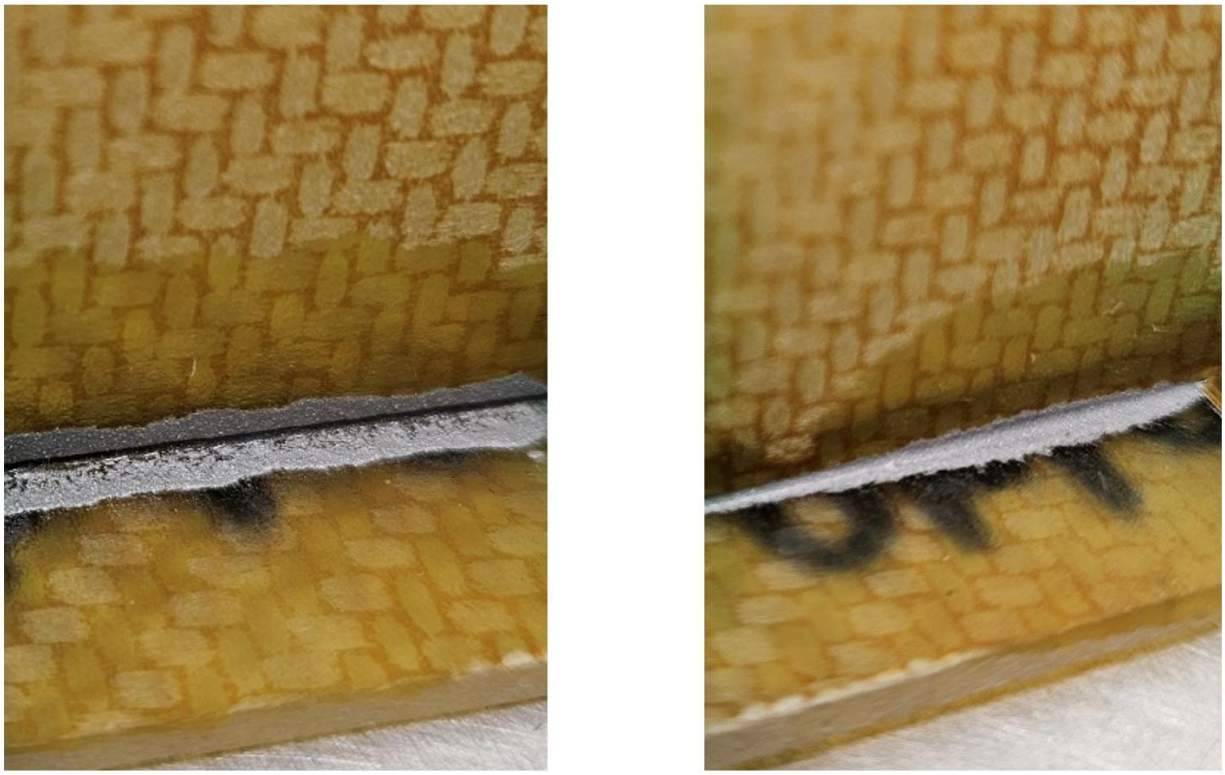

Figure 16: Adheive joint on the upper side (left) and the underside (right) after curing with 0.40 mm glue gap. The joint has flowed down too much and created an “undercut” on the upper side and formed a radius on the underside.

To achieve repeatability in the amount and placement of adhesive a robot was used for dispensing. Several trials were conducted to find the optimal adhesive amount and application pattern. By using a transparent ring, the spread of glue after compression was observed. This is depicted in Figure 17.

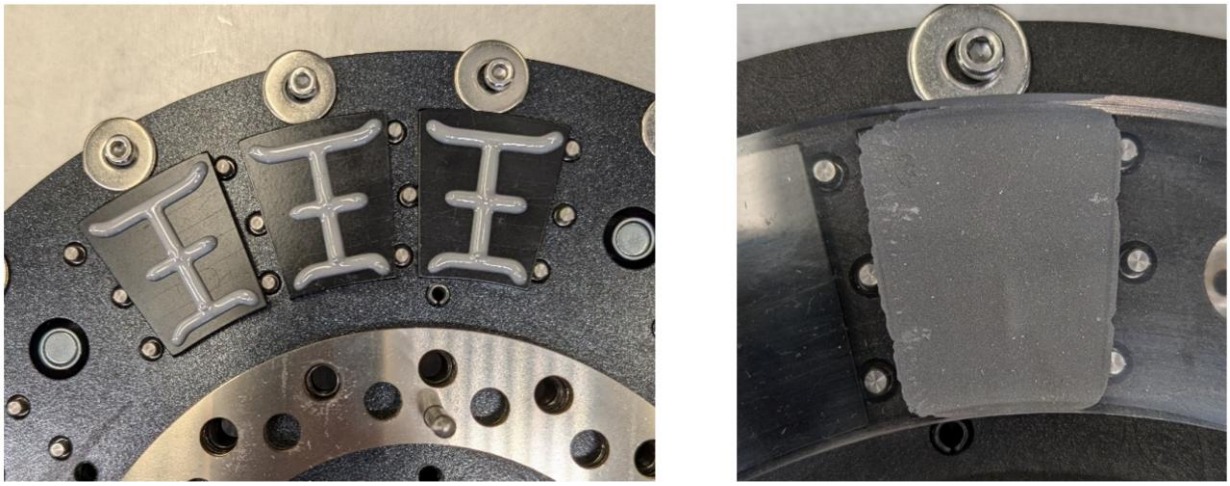

Figure 17: Adhesive pattern and amount trial

To control the adhesive gap thickness measurement sticks (Plastigauge) were used to measure the gap, and shims were used to adjust the gap before application of adhesive. Several tests were also performed to understand the impact of different temperature profiles during curing as this can have a significant impact on how the glue flows, thermal expansion of the different components and the temperature at which the adhesive cures.

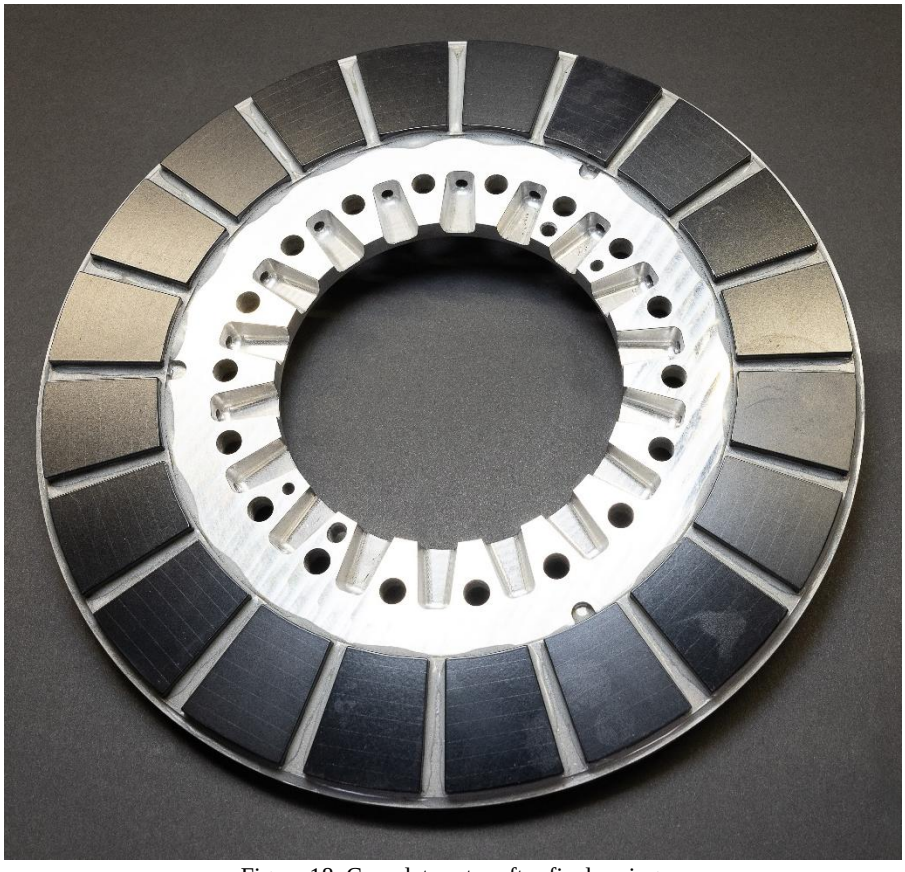

Figure 18: Complete rotor after final curing.

2.2.2 **Rotor burst test**

To verify the rotor design in general and the adhesive strength specifically a burst test was performed where the rotor speed was increased until failure, the assembly is depicted in Figure 19. The burst test was performed with the complete rotor heated to 85°C to capture the reduction in adhesive strength as well as stresses due to thermal expansion.

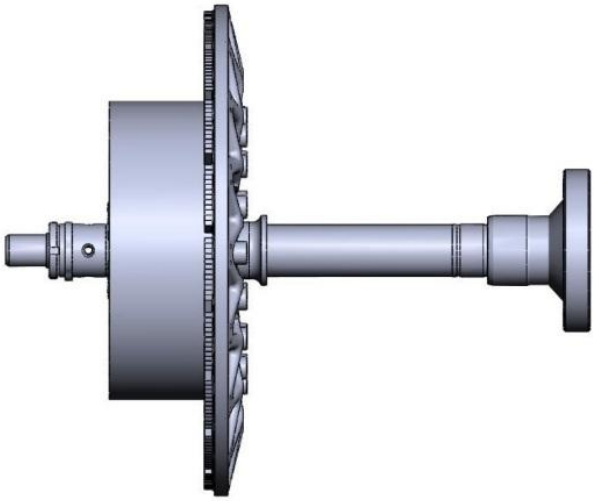

Figure 19: Rotor assembly used in the burst test.

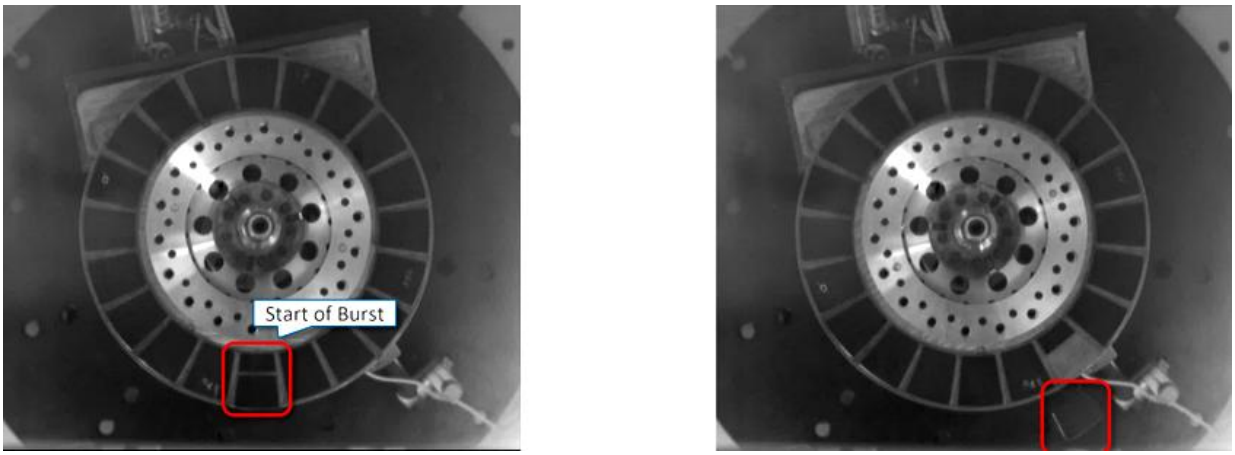

Figure 20: High speed camera frames from the burst (one magnet) at 12.900 rpm.

The burst speed of 12900 rpm, as depicted in Figure 20. Comparing the burst speed to the maximum operational speed of 9000 rpm, gives a stress safety factor 2, which was judged sufficient for a prototype build. The safety factor would likely need to be increased for a volume production intent design due to thermal and mechanical fatigue as well as component and process variations.

2.3 Stator

The stator is made from an aluminium housing, individual teeth, winding, and glass-fibre reinforced epoxy components. An adhesive applied by a robot is used for bonding the components together. Finally, the stator is impregnated to provide mechanical fixation of the winding and for additional insulation. Different alternatives for the stator soft magnetic material were considered, NO35, GO20 and SMC. Although GO20 gives higher efficiency due to lower iron losses and higher torque due higher permeability SMC was selected due to the better design flexibility. This is especially important for the design of the tooth tips which helps to reduce the winding AC-losses at high speed operation and reduce torque ripple. The winding is a concentrated winding with rectangular wire made by coil bending followed by laser welding and powder coating. Special efforts were made to make the design suitable for production and future scaling to mass production. As a result, the welds are all in one plane and can be welding in equipment similar to conventional hairpin welding. The welds also stick out to enable an efficient process for the weld insulation using epoxy powder coating similar to conventional hairpin windings, see Figure 21.

Figure 21: Winding before assembly in the stator.

2.3.1 Stator cooling

To reach high power and torque density the stator is directly oil cooled. Nominal oil flow was specified to 12 l/min with 60°C inlet temperature. To understand and optimize the oil cooling several iterations using CFD simulations for a few selected operating points.

The stator losses consist of iron losses in the SMC teeth and winding losses. The winding losses were further broken down to DC-Losses and AC-Losses as these are unevenly distributed between the turns in the winding and risks creating hotspots. From the electromagnetic simulations in JMAG the losses were extracted for 5 zones of turns for each coil according to the Table 3 and Figure 22.

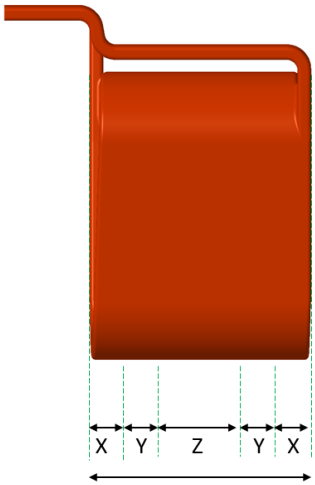

Figure 22:coil loss zones for one coil. Total number of turns is 14 per coil.

Table 3: loss per coil winding zone for three selected operating points. Zone X and Y consist of 2x2 turns each. Zone Z consists of 6 turns. Losses especially at higher speeds are significantly higher per turn in zone X. In the 9000 rpm operating point for example zone X losses are 62% higher than in zone Z.

Loss Zone / Operating Point	**2785 rpm & 251 Nm**	**3342 rpm & 413 Nm**	**9000 rpm & 80 Nm**
Zone X [W]	15.7	53.7	51.2
Zone Y [W]	11.8	42.4	23.7
Zone Z [W]	33.6	117.3	38.7
Total [W]	88.6	307.5	188.6

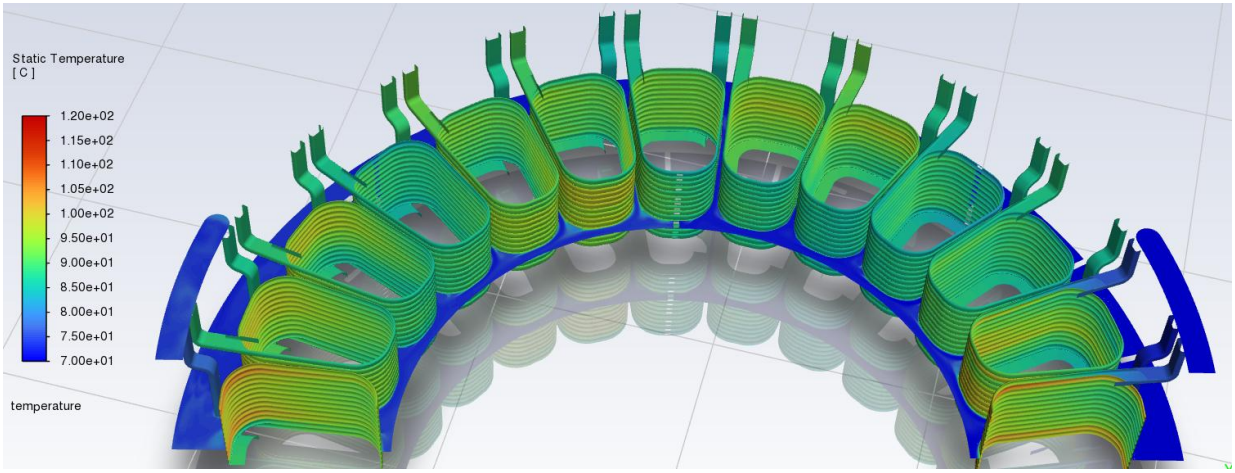

Figure 23: temperature distribution in the windings for the 2785 rpm & 251 Nm load case after optimization of the flow. Hot spots are at around 120°C, which is about 50°C lower than before optimizations.

In order to get an even flow plastic flow blockers and diverters were added in selected locations around the windings in the stator housing. This has resulted in a simulate temperature distribution as depicted in Figure 23.
An assembly fixture was developed and build to enable a controlled assembly of the machine. The steps where the magnetized rotors are lowered against the stator is especially critical due to the very high magnetic forces (several kN) involved. The final result is depicted in Figure 24.

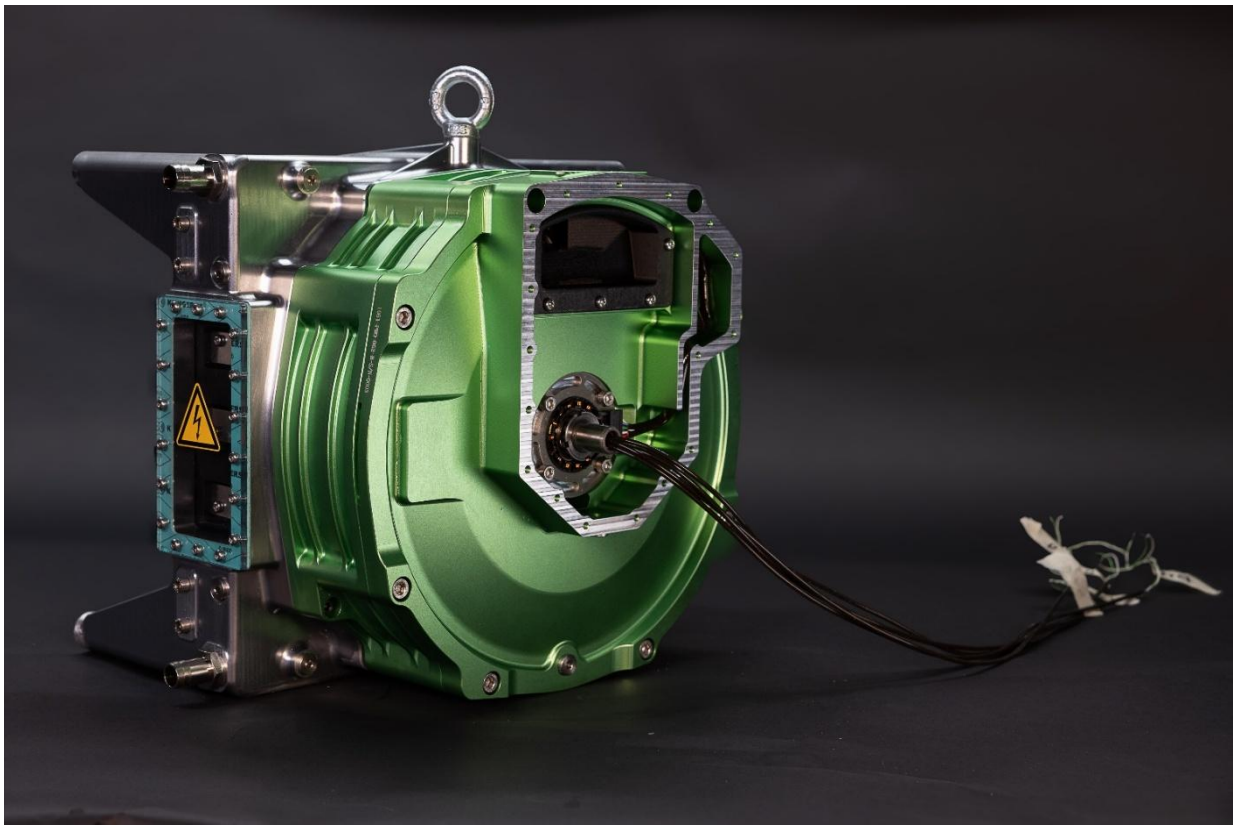
Figure 24: The completed axial machine on a test stand.

3 Results and conclusions

Design and manufacturing of axial flux automotive traction machines is indeed very challenging. By using an approach starting with simulations and a digital twin combined with an iterative approach where simulation results, previous experience, sub-system and component test results and supplier input are fed back in the design it has been shown that it's possible to design and build a machine while navigating around the major pitfalls. All learnings are continuously fed back into our lessons learned and design guideline documents to be ever better prepared for the next challenging project. Taking an axial flux machine into mass production poses further challenges in many areas. The list of new ideas, improvements and innovations created during this project would serve as a good starting point for meeting those challenges.

References

[1] Chalmers, B.J., Spooner, E., & Haydock, L. (1992). "'TORUS' : A slotless, toroidal-stator, permanent-magnet generator." IEE Proceedings B - Electric Power Applications, 139, No 6, 497-506.

[2] JMAG Simulation Software. (2023). Comprehensive Electromagnetic Design Tools for Electrical Machines. Available at: https://www.jmag-international.com.

Presenter Biography

Kristoffer Nilsson has an M.Sc. in Mechanical Engineering from Linköping University. He has been working in the field of electric traction systems for vehicles for 15 years.